Science of the Total Environment 639 (2018) 1530–1542

Contents lists available at ScienceDirect

Science of the Total Environment

journal homepage: www.elsevier.com/locate/scitotenv

Activated magnetic biochar by one-step synthesis: Enhanced adsorption and coadsorption for 17β-estradiol and copper

Zhihong Yin [a,b], Yunguo Liu [a,b,*], Shaobo Liu [c], Luhua Jiang [a,b], Xiaofei Tan [a,b], Guangming Zeng [a,b], Meifang Li [a,b], Sijia Liu [a,b], Sirong Tian [a,b], Ying Fang [a,b]

[a] College of Environmental Science and Engineering, Hunan University, Changsha 410082, PR China
[b] Key Laboratory of Environmental Biology and Pollution Control (Hunan University), Ministry of Education, Changsha 410082, PR China
[c] School of Architecture and Art, Central South University, Changsha 410082, PR China

HIGHLIGHTS

- AMBCs were synthesized via one-step activation, magnetization and carbonization process with different pyrolysis temperature.
- AMBCs have the large specific surface area and more contained oxygen functional groups compare to pristine biochar.
- The maximum adsorption capacities of AMBC-700 and AMBC-300 were 153.20 and 85.93 mg/g for E2 and Cu(II), respectively.
- There exists site competition and enhancement of E2 and Cu(II) on the sorption by AMBCs in binary-solute system.

GRAPHICAL ABSTRACT

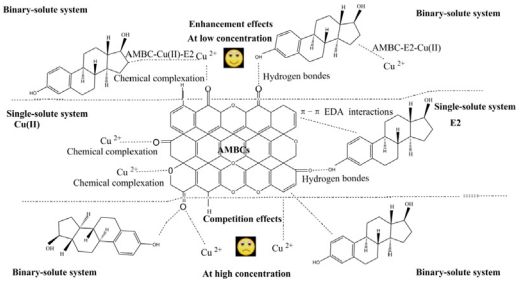

ARTICLE INFO

Article history:
Received 4 February 2018
Received in revised form 18 April 2018
Accepted 10 May 2018
Available online xxxx

Editor: Baoliang Chen

Keywords:
Activated magnetic biochars
One-step
17β-estradiol
Copper
Adsorption
Coadsorption

ABSTRACT

In this study, activated magnetic biochars (AMBCs) were successfully synthesized via one-step synthetic method with different temperature (300, 500 and 700 °C). Characterization experiments indicated that AMBCs had larger surface area, higher pore volume and more contained oxygen functional groups compared to the pristine biochar. In addition, AMBCs showed better adsorption performance for 17β-estradiol (E2) and copper (Cu(II)) in single/binary-solute systems than unmodified pristine biochar. AMBC-700 exhibited the highest capacity (153.2 mg/g) for E2, while the AMBC-300 showed the best adsorption capacity (85.93 mg/g) for Cu(II) in single-solute system. Adsorption of Cu(II) and E2 both followed by pseudo-second-order and Langmuir isothermal model. The initial pH of the solution had an effect on the adsorption of E2 and Cu(II) in single-solute system. Coadsorption experiments indicated that there existed site competition and enhancement of E2 and Cu(II) on the sorption in binary-solute system. Results from this study indicated that the E2 was adsorbed by hydrogen bonds, π-π EDA interactions. Cu(II) was mainly adsorbed via chemical complexation between contained oxygen functional groups and Cu(II) ions. Therefore, the AMBCs via one-step synthesis could be converted into value-added biochar as effective sorbent for simultaneous removal of E2 and Cu(II) from water.

* Corresponding author at: College of Environmental Science and Engineering, Hunan University, Changsha 410082, PR China.
E-mail address: hnuliuyunguo@gmail.com (Y. Liu).

https://doi.org/10.1016/j.scitotenv.2018.05.130
0048-9697/

1. Introduction

Endocrine disrupting chemicals (EDCs) and heavy metals pollution have become public concern due to their threat to the aquatic environment and human beings (Jiang et al., 2017; Jiang et al., 2016; Wang et al., 2015; Zhang and Zhou, 2005; Zhou et al., 2018). 17β-estradiol (E2), as one of the EDCs, is widely detected in the ground water and surface water (Fan et al., 2013; Johnson et al., 2013). Copper (Cu(II)) is an harmful heavy metal and is defined as a priority by united states environmental protection agency (US EPA) (Yang and Jiang, 2014). It has been reported that Cu(II) has strong complexation ability with organic pollutants (Y. Sun et al., 2014), which likely interacted with each other and consequently led to harmful effects on organisms and human beings. Hence, considering this disadvantages of E2 and Cu(II) in the water, it is of great importance to look for an efficient remediation technology for the simultaneously removal of E2 and Cu(II) from water.

Various technologies such as adsorption (Li et al., 2017b; Wang et al., 2015), photodegradation (Atkinson et al., 2011), catalytic degradation (Qin et al., 2015), biodegradation (Bradley and Writer, 2014) and reduction (Zhou et al., 2016) have been often employed in removal EDCs and heavy metal. Adsorption is considered as the good choice because of low cost, simple design and generation. A number of sorbent materials have been applied for E2 and Cu(II) removal, such as biochar (Li et al., 2017a), multi-walled carbon nanotubes (Sun and Zhou, 2014) and other nanomaterials (Zhao et al., 2011). Among these materials, biochar are widely used as an adsorbent for wastewater treatment because of cheap, low environment impact and efficient (Tan et al., 2016; Tan et al., 2015; Zhao et al., 2017). However, the application of biochar was limited (Reddy and Lee, 2014). If the biochar after adsorption is not separated in time, which may generate the risk of secondary pollution. Therefore, it is necessary to improve the adsorption properties of biochar in practice application.

Magnetic biochars derived from waste biomass have been widely studied in environmental applications because of they have shown promising performance for pollutants and could be easily separated from solution using a magnetic separator (Jung et al., 2016; M. Li et al., 2013; Y. Li et al., 2013; Mohan et al., 2011). There are several procedures for introducing magnetic particles into biochar, including microwave irradiation (Gollavelli et al., 2013), hydrothermal coprecipitation reaction (Nethaji et al., 2013) and simultaneous carbonization (Wu et al., 2014). However, microwave irradiation is frequently consumed-time and complex. The magnetic biochar prepared from the hydrothermal coprecipitation reaction is unstable under an acidic condition. The simultaneous magnetization and carbonization can be facile fabricated via pyrolysis of Fe loaded biomass materials. However, the specific surface area (SSA) and pore volume of the magnetic biochar cannot be enhanced effectively due to the negative effect of the magnetic medium. As reported, chemical activation could significantly enhance the SSA and the porous structures of biochar by formation of the well-developed porosity (Angin et al., 2013; Zhu et al., 2014). Angin et al. (2013) reported that the SSA and internal pore structures of biochar by chemical activation are greatly enhanced compared to pristine biochar. Chen et al. (2016) research showed the SSA of biochar by chemical activation reached 1057.8 m^2/g. Hence, it is expected that high performance biochar can be synthesized by simultaneous activation, magnetization and carbonization.

Activation and magnetization are two important methods in biochar study. However, the magnetization of biochar is often separated from the activation method (Bastami and Entezari, 2012; B. Han et al., 2015). In fact, such one-step activation, magnetization and carbonization process can significantly reduce the numbers of steps for the preparation process and result in biochar more attractive as adsorbents for removing pollutants from aqueous solution. The surface properties of biochar can be simultaneously enhanced both physically and chemically via one-step synthesis method. Nevertheless, there are little information about the biochar produced by one-step activation, magnetization and carbonization for the simultaneous removal of E2 and Cu(II) from water.

In this paper, activated magnetic biochars (AMBCs) has been prepared by one-step facile method for use in E2 and Cu(II) removal from water. The rice straw was selected as the raw material of biochar. The specific purposes of the current study were aim to (1) prepare AMBCs via one-step activation, magnetization, and carbonization with different temperatures (300, 500 and 700 °C). Activated biochar (ABC), magnetized biochar (MBC) and raw biochar (RBC) samples were also prepared as a contrast. (2) Investigate the adsorption capacity of AMBCs for E2 and Cu(II) in single/binary-solute system. (3) Explore the effect of pH on adsorption process of E2 and Cu(II) in single-solute system. (4) Explore the effect of coexisted E2/Cu(II) on individual adsorption in binary-solute system. (5) Investigate the potential mechanisms of E2 and Cu(II) onto AMBCs. This present study supplied new insights in the development of biochar and advances their applications in water treatment.

2. Materials and methods

2.1. Main reagents and solutions

E2 (purity = 98.0%, molecular weight 228.29) was purchased from Sigma-Aldrich Corporation. A stock solution of E2 used in batch experiments was prepared by dissolving 0.125 g of E2 powder into 50 mL methanol solution. The desired E2 concentration used in this experiment were obtained by diluting the stock solution with deionized water (18.2 MΩ/cm). Rice straw was collected from the farm of Yiyang, Hunan province, China. A stock solution of Cu(II) was prepared by dissolving 1 g of $Cu(NO_3)_2 \cdot 3H_2O$ in 1000 mL deionized water. All other chemicals were analytical grade and were purchased from Shanghai Chemical Corporation. All solutions were prepared with deionized water.

2.2. Preparation of AMBCs by one-step synthetic method

The AMBCs were prepared from modified Wang et al. method (Wang et al., 2017). The procedure for the preparation was as follows: rice straw were washed with deionized water and dried, then passed through a 100-mesh sieve and collected. 2 g of $ZnCl_2$ and 2 g of $FeCl_3 \cdot 6H_2O$ were added to 500 mL of deionized water and mixed uniformly. Then, 10 g of rice straw power was added to the mixed solution. Next, the mixed solution was sonicated for 2 h and then immersed for 24 h, and finally dried at 80 °C. The collected particles were placed in a tubular resistance furnace. The temperature in the furnace was increased to design temperature (300, 500 and 700 °C) and then maintained for 1 h. Generally, the biochar yield decreases with increasing in pyrolysis temperature. The pyrolysis temperature has influence on pore volume and surface area of biochar. An increase of the pyrolysis temperature results in an increase of the carbon content in biochar. This increase is especially pronounced in the temperature range from 300 to 500 °C. Setting pyrolysis temperature higher than 700 °C does not seem appropriate to generate biochars with higher adsorption capacity (Manya, 2012). However, if the pyrolysis temperature is lower than 200 °C, biochar cannot be carbonized completely. In order to investigate the effect of pyrolysis temperature, this work synthesized the AMBCs with three different temperature (300, 500 and 700 °C). After pyrolysis, samples were naturally cooled to room temperature, and then were washed with deionized water to neutral and dried at 85 °C. Finally, the obtained samples were collected and referred to as AMBC-300, AMBC-500, AMBC-700, respectively, where the suffix number represented the pyrolytic temperature. For the contrasts, the activated biochar (ABC), magnetized biochar (MBC), and raw biochar (RBC) were also prepared by the single activation, magnetization and carbonization process at 300 °C, respectively. The preparation process is schematically exhibited in Scheme 1.

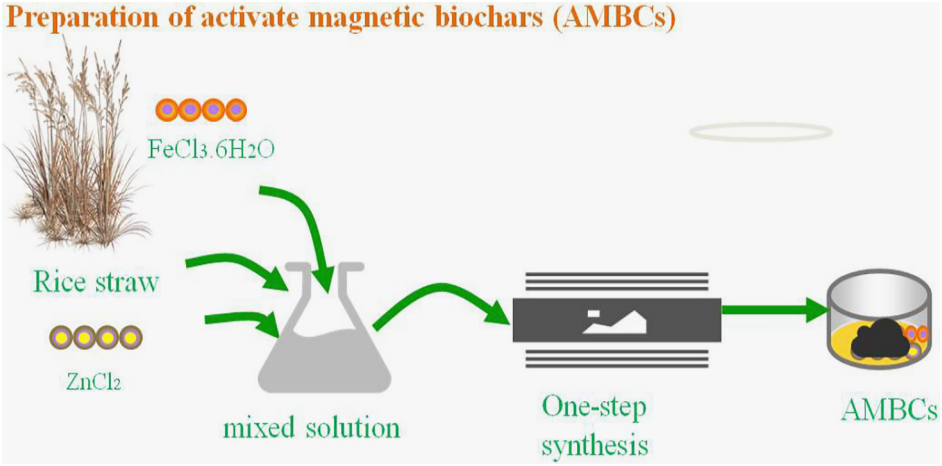

Scheme 1. Schematic representation of preparation process of the AMBCs.

2.3. Characterization

The surface morphologies of biochar materials were characterized by the field emission scanning electron microscope (SEM, Quanta-400, USA), transmission electron microscopy (TEM, Tecnai G2 F20, USA) and the energy dispersive X-ray spectroscopy (EDS). The SSA, total pore volume, average pore width and average particles size of biochar samples were measured by N_2 adsorption-desorption isotherm at 77.3 K using a Micromeritics TriStar II 3020. The elemental composition of the product was recorded by an elemental analyzer (Vario EL III, Elementary, Germany). The zeta potential of all samples was measured at pH 2.0–11.0 with a zeta potential meter (Zetasizer nano-ZS90 Malvern). To investigate the surface chemical properties, the Fourier transforms infrared (FTIR) spectrophotometer for all samples recorded between 500 and 4000 cm^{-1} (Nicolet 6700 spectrometer, USA). The structure and crystallinity of the sorbent were characterized on an X-ray diffractometer (XRD) (D/max-2500, Rigaku, Japan) with Cu Kα radiation at 40 kV and 30 mA in a 2θ range of 10–60°. Magnetic properties of the samples were measured with a vibrating sample magnetometer (VSM, Mpms (squid) XL-7, Quantum, USA) at room temperature. The surface functional groups and chemical composition of biochars were analyzed by X-ray photoelectron spectroscopy (XPS).

2.4. Batch adsorption and coadsorption experiments

Single-solute system: batch experiments were conducted by adding biochars (5 mg for E2, 40 mg for Cu(II)) and pollutants solution (100 mL for E2, 50 mL for Cu(II)) to a 150 mL glass vial. The initial concentrations of E2 (1–8 mg/L), Cu(II) (20–140 mg/L) solutions were controlled to achieve the desired equilibrium concentration. Effect of initial solution pH on E2 and Cu(II) adsorption was investigated at different pH. The pH was adjusted to desired values via adding negligible volumes of NaOH and HCl solution. Then, the mixed solutions were stirred continuously at 150 rpm for 24 h until reached equilibrium. Then, the solid/liquid phases of MBC, AMBC-300, AMBC-500, AMBC-700 were separated by a permanent magnet. The solid/liquid phase of RBC and ABC after centrifugation at 2500 rpm for 10 min, were filtered by syringe filter (0.45 μm polypropylene membrane).

Binary-solute system: the coadsorption of E2 and Cu(II) were carried out by batch experiments. Other than the addition of different initial concentration of Cu(II) (10, 20, 30, 40, 50 and 60 mg/L) in the E2 (6 mg/L) solutions, and the addition of various initial concentration of E2 solutions (1, 2, 3, 4, 5 and 6 mg/L) in the Cu(II) (140 mg/L) solutions, all conditions were identical to the single-solute system adsorption experiments mention above.

The final concentration of E2 solution was measured by an F-4500 fluorescence spectrophotometer (Hitachi, Japan). The Cu(II) residues were determined using atomic adsorption spectroscopy (PerkinElmer AA700, USA). The adsorption of the E2 and Cu(II) at equilibrium per unit mass of biochar were calculated according to the following equation.

$$q_e = \frac{(C_o - C_e) \times V}{m} \quad (1)$$

where q_e (mg/g) is the adsorbed amount at equilibrium. V (L) is the volume of the solution. m (g) is the mass of adsorbent. C_0 (mg/L) is the initial concentration of pollutant. C_e (mg/L) is the equilibrium concentration of the adsorbate in solution. All adsorption experiments were conducted at room temperature and three replicates were used for each treatment as controls.

2.5. Regenerated experiments

Adsorption-desorption experiment was carried out as the following: the AMBCs which have been used to removal E2 and Cu(II) were rinsed repeatedly with 100 mL ethanol solution and deionized water at room temperature. After desorption, the suspension liquid was taken to separation by a permanent magnet. And the final samples was dried at 353 K for reuse. In each cycle of adsorption-desorption test, the recycled AMBCs were added into 100 mL 6 mg/L E2 and 50 mL 140 mg/L Cu(II) solution, respectively. Then the mixed solution was shaken at 298 K to reach adsorption equilibrium.

3. Results and discussion

3.1. Basic properties of biochars

3.1.1. Morphologies, BET surface area and elementals analysis

The morphological features of biochar materials were characterized by obtaining SEM images, as shown in Fig. 1. It was clearly seen that the AMBC-300, AMBC-500 and AMBC-700 possessed some cracks and porosity in their surface structure. The EDS of adsorption materials are also exhibited in Fig. S1. The EDS results confirmed the composition including carbon, nitrogen, oxygen, and iron, which indicated that the AMBCs was successfully synthesized by one-step methods. The biochar materials were also examined by the TEM images, as displayed in Fig. S2. It was obvious that there was a large number of small particles dispersed on the surface of the AMBCs, which were presumably iron oxide nanoparticles.

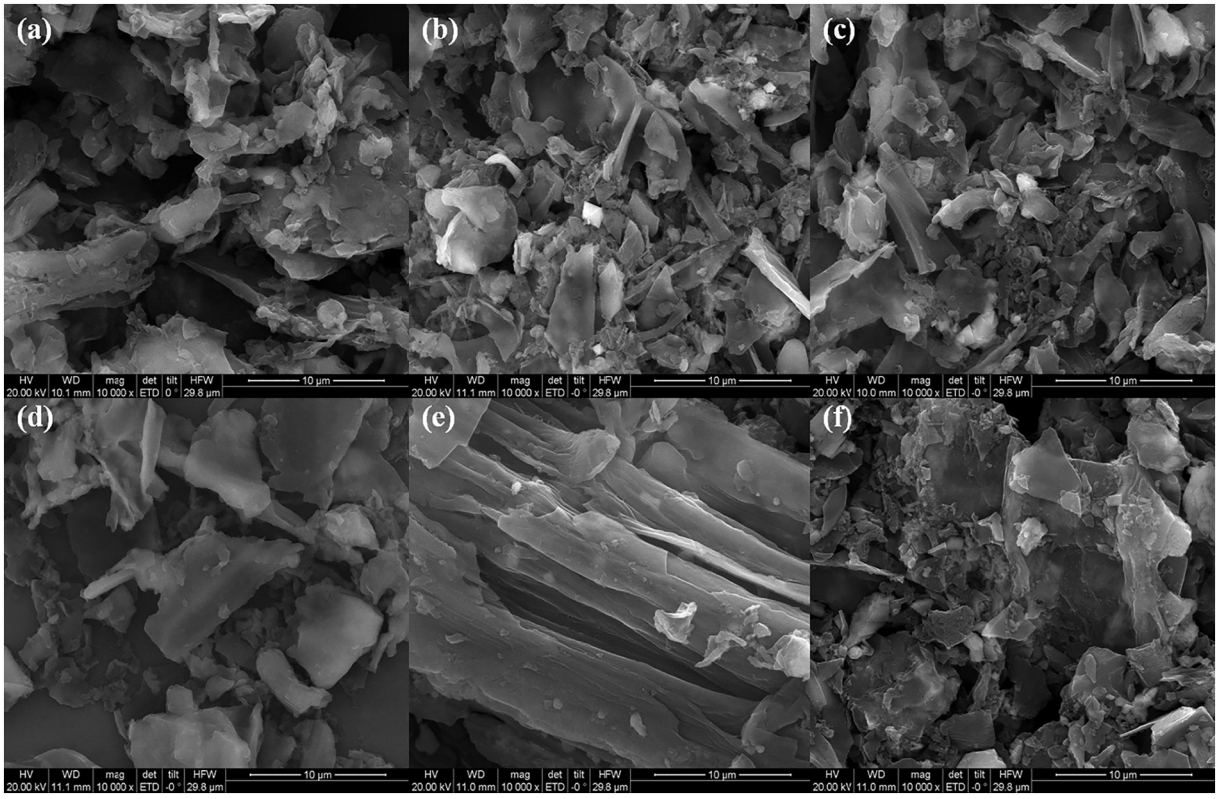

Fig. 1. The SEM images of RBC (a), MBC (b), ABC (c), AMBC-300 (d), AMBC-500 (e), and AMBC-700 (f).

The SSA, elementals, XPS and zeta potential measurements were used for the characterization of various biochars, and the results are shown Table 1. The SSA values of RBC, MBC, ABC, AMBC-300, AMBC-500 and AMBC-700 were found to be 64.9, 183.9, 243.47, 263.21, 276.03 and 357.84 m^2/g, respectively, which indicated that SSA of modified biochars were larger than that of unmodified biochar. The SSA value of AMBC-700 was 5.51 times than that of RBC. Thus, the one-step activation, magnetization and carbonization process could be considered to be effective in preparing biochar with highly porous. This phenomenon could be ascribed to the fact that the activation process improved the development of pores and created new pores, resulting in the increases in the SSA of biochar (Lua and Yang, 2004). Furthermore, the SSA values of modified biochar increased with increasing pyrolysis temperature. The SSA values of AMBC-700 increased by 35.95% and 29.64% compared to AMBC-300 and AMBC-500, respectively. It is worth noting that the SSA of AMBCs materials were higher slightly than that of some related materials reported by similar methods. For example, the activated, magnetic biochars synthesized by Cazetta et al. (2016) using coconut shells showed SSA values between 238 and 337 m^2/g. Additionally, the SSA values of AMBCs materials were much high than other biochar prepared by other methods. For instance, the surface area of hydrochar-biochar prepared by Fe-Mn binary oxide modified hydrochar process by Ning et al. (2017) is only 167.17 m^2/g. Generally, relatively high SSA of the adsorbents could achieve a better adsorption performance.

The elementals analysis of various biochar samples are also presented in Table 1. As seen, the biochar materials contain carbon, nitrogen, oxygen and hydrogen elements. Carbon and oxygen are one of the major elements of biochar. The content of carbon were in the following order: AMBC-300 (82.18%) > AMBC-500 (78.54%) > AMBC-700 (75.89%) > ABC (73.33%) > MBC (62.46%) > RBC (61.06%). The carbon content of modified biochar was higher than that of unmodified biochar. The results could be explained that the release of volatiles during carbonization that enhances the elimination of non carbon species and enrichment of carbon (Z. Han et al., 2015). As the pyrolysis temperature increased, the carbon content of AMBC-700 was less than that of AMBC-500 and AMBC-300. In addition, the oxygen content of modified biochar were in the following order: AMBC-300 (10.50%) > AMBC-500 (9.85%) > AMBC-700 (9.83%) > ABC (9.09%) > MBC (8.30%) > RBC (7.78%), which indicated that the oxygen content of modified biochar was higher than that of the pristine biochar. The phenomenon could cause by the formation of contain oxygen functional groups. The oxygen

Table 1
Selected physiochemical properties of RBC, MBC, ABC, AMBC-300, AMBC-500 and AMBC-700.

Adsorbent	XPS				Basic features			pHpzc	Organic elemental analysis			
	C(%)	N(%)	O(%)	Fe(%)	BET surface area (m^2/g)	Pore volume (cm^2/g)	Pore size (nm)		C(%)	H(%)	N(%)	O(%)
RBC	81.36	2.69	9.26	–	64.90	0.04	2.68	3.25	61.06	2.43	1.47	7.78
MBC	83.58	2.82	10.48	1.22	183.90	0.08	1.75	4.56	62.46	2.42	1.49	8.30
ABC	83.99	3.06	11.01	–	243.47	0.11	1.66	4.05	73.33	2.28	1.48	9.09
AMBC-300	86.32	3.00	13.56	1.23	263.21	0.11	1.84	4.25	82.18	2.31	1.48	10.50
AMBC-500	85.69	3.01	12.85	1.24	276.03	0.14	1.99	4.55	78.54	2.21	1.47	9.85
AMBC-700	85.31	2.76	12.07	1.25	357.84	0.22	2.25	6.26	75.89	1.23	1.40	9.83

and carbon content decreased with increasing pyrolysis temperature, which could be explained by the amount of contained oxygen functional groups decreased with the increase in temperature.

3.1.2. Zeta potential and N_2 adsorption-desorption analysis

The point of zero charge (pH_{pzc}) of six kinds of biochar is shown in Table. 1. As seen, the pH_{pzc} values of RBC, MBC, ABC, AMBC-300, AMBC-500 and AMBC-700 were 3.25, 4.56, 4.05, 4.25, 4.55, and 6.26, respectively. The pH_{pzc} values of modified biochar (AMBC-300, AMBC-500, and AMBC-700) were higher than that of RBC, and the pH_{pzc} of AMBC-300, AMBC-500, and AMBC-700 increased gradually from 4.25 to 6.26 as increasing pyrolysis temperature. This result was likely caused by the surface coverage with maghemite (mainly $FeOH_2^+$), since the pH_{pzc} of maghemite were about 6.5 or higher (B. Han et al., 2015; Lucas et al., 2007), thus resulting in the pH_{pzc} values of modified biochar increased. Moreover, the values of pH_{pzc} were close to other relative materials that was reported in the previous literature (Cazetta et al., 2016).

Fig. 2a shows the N_2 adsorption-desorption isotherms plot of all biochar samples. According to IUPAC classification, this clearly indicated that the isotherm curves of RBC and MBC were found to be as type I, which was characteristic of microporous materials (Angin et al., 2013). The isotherm for ABC, AMBC-300, AMBC-500 and AMBC-700 could be classified as type IV, which were characteristic of mesoporous materials (Cazetta et al., 2016). Moreover, there was significant volume of N_2 adsorbed by the AMBC-700 at high relative pressure, which might be due to the presence of lots of mesopores on AMBC-700 surface. Further confirmed by the pore size distributions are shown in Fig. 2b. The AMBCs materials especially AMBC-700 showed more mesoporous and macroporous structures than RBC. It can be seen that one-step synthesis resulted in significant microporosity and mesoporous development. In fact, the functional groups of biochar could react with $ZnCl_2$ and form water vapor during the process of pyrolysis and activation. Therefore, water vapor reacted with the carbon of biochar, resulting the formation of internal pore structure. A study conducted by Sun et al. (2015) confirmed that the contained oxygen functional groups could decompose to gaseous H_2O and CO_2 and then led to form a pore structure after H_2PO_4 activation. Similarly, the activation process of $ZnCl_2$ modified biochar, resulting in the formation of pore structure. Therefore, one-step synthetic process could enhance the development of microporous and mesoporous structures on biochar.

3.1.3. The FTIR and XRD analysis

Fig. 2c shows the FTIR spectra of RBC, MBC, ABC, AMBC-300, AMBC-500, and AMBC-700, respectively. The spectra for biochar samples appear similar, revealing their similar compositions. The peak of 3435 cm^{-1} could be ascribed to the hydrogen bonded O—H stretching vibrations, which indicated the presence of hydroxyl (Unur, 2013). The peak of 1390 cm^{-1} was assigned to the appearance of carboxyl bonds (O═C—O) (Jung et al., 2016). The band at 1029 cm^{-1} could be assigned to C—O stretches in both hydroxyl and carboxylate moieties (Sevilla and Fuertes, 2009). The band at 2923 cm^{-1} could be ascribed to the stretching vibration of aliphatic C—H (Sevilla and Fuertes, 2009). The bands at 1700 and 1607 cm^{-1} could be attributed to C═O and C═C vibrations, respectively, which indicated the aromatization of the biochar (Zhu et al., 2014). One new peak of 1418 cm^{-1} for ABC was observed.

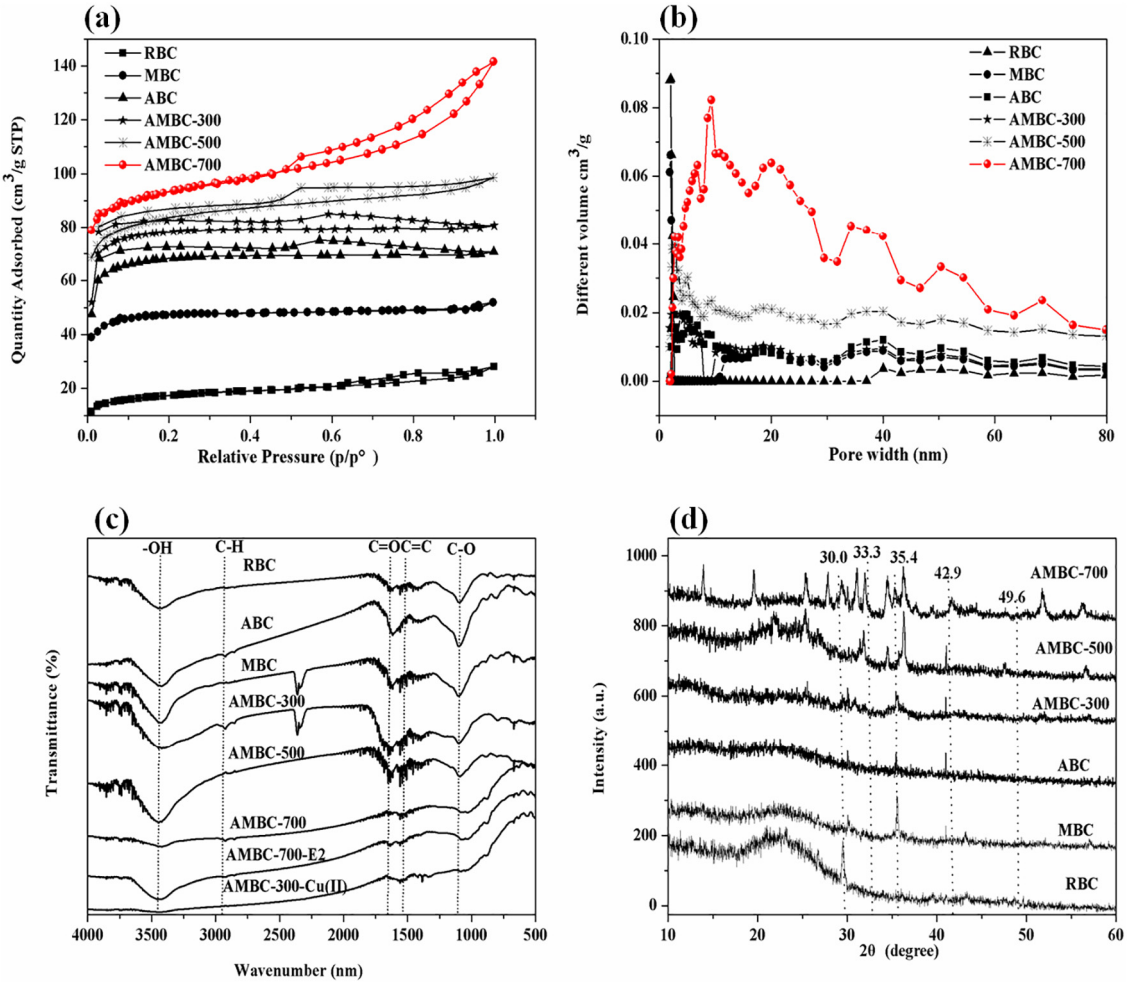

Fig. 2. The nitrogen adsorption-desorption isotherms (a), the pose size distributions (b), FTIR spectra (c) and XRD pattern (d) for RBC, MBC, ABC, AMBC-300, AMBC-500, and AMBC-700.

This peak was attributed to the carbonyls ion groups, which was formed properly because of the extraction of hydrogen element and O—H groups from aromatic rings as a results of the effect of $ZnCl_2$ (Sahu et al., 2010). The above results indicated that the functional groups on the surface of biochar samples increased via one-step activation, magnetization and carbonization process. There are some oxygen-containing functional groups on the surface of modified biochar such as hydroxyl and carboxyl groups, which might be resulted in an increase of adsorption capacity due to its could provide some adsorption sites for them.

The structure and phase composition of biochar samples characterized by powder XRD pattern are presented in Fig. 2d. As seen, it is possible that two different crystal phases exist in the biochar: magnetite and hematite. The magnetite was a crystalline oxide whereas hematite was a crystalline solid with hexagonal compact structure. The peaks of 30.0, 35.4 and 42.9° corresponded to the 220, 311 and 400 basal planes of the crystalline magnetite portion of the biochar (Xiao et al., 2013). The peaks of 33.3 and 49.6° were characteristics of the 104 and 024 basal planes of the hematite portion of the materials (Varshney and Yogi, 2011). Furthermore, the magnetite portion of the materials was seen to have higher degree of crystallinity. The results indicated that the iron ions were successfully loaded on the surface of the biochar, which provided the conditions for biochar magnetic separation. Such iron oxides species such as hematite, magnetite are expected to form from the hydrolysis of $FeCl_3$ in aqueous solution, in a process involving the formation of mono-, di- and polynuclear iron hydroxide species, which might be the formation of AMBCs. Specifically, the activation process of $ZnCl_2$ caused the formation of stable structure, such as C═C, C═O and O═C—O bonds, due to the breaking of unsaturated bonds. Additionally, there was another member of iron oxides family called maghemite, which has a similar structure as that of magnetite. It was difficult to discern the magnetite phase from the maghemite phase by XRD alone. Hence, XPS spectroscopy was used to distinguish between the two components, as showed below and in the Supporting Information section.

3.1.4. The magnetization properties and XPS analysis

The magnetization hysteresis curve of AMBC-300 and AMBC-700 were obtained by using VSM at room temperature and the results are displayed in Fig. 3. Specific pertinent data showed ferromagnetic properties with saturation magnetization (M_s) values of 0.003396 and 0.002242 emu/mg for AMBC-300 and AMBC-700, respectively, which indicated that AMBC-300 and AMBC-700 was enough to realize solid-liquid separation by using a permanent magnet. The values of coercivity (H_c), remanence (M_r) and the ration remanence and saturation magnetization (M_r/M_s) are listed in Table S1. Based on the results, it is possible to conclude that the AMBC-300 and AMBC-700 possess superparamagnetic properties as their rations of M_r/M_s were found to be less that 25% (Ranjithkumar et al., 2014). Furthermore, the separation performance of AMBC-700 could be demonstrated by the insets displayed in Fig. 3, which indicated that the AMBCs could be separated from the treatment solution via a permanent magnet. Therefore, the magnetization process makes biochar more easier separation from the following treatment solution.

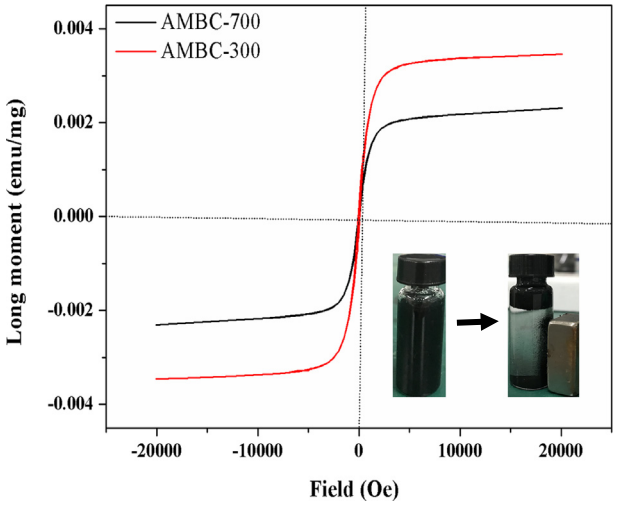

Fig. 3. Magnetic hysteresis loops of AMBC-300 and AMBC-700.

To get an insight into the surface properties, the surface elemental composition of biochar samples were further characterized by means of XPS. Fig. S3 showed the XPS survey spectra of the all biochars. On the basic of the results, the biochar materials contain carbon, nitrogen, oxygen and iron elements. The elemental compositions of the biochars obtained from XPS spectra are also displayed in Table 1. The results showed that AMBC-300 had the highest amount of O (13.56%) and C (86.32%), which consistent with the results of elemental analysis. Fig. 4 shows the XPS peak deconvolution for C 1s spectra of biochar samples. Specifically, the peak of 284.7 and 285.0 eV were assigned to C═C and C—C bonds, respectively. The peak of 286.5 eV was contributed to C—OH. Other peaks of 287.3 and 289.5 eV were ascribed to C—O—C and —COOH, respectively (Akhavan et al., 2013). Fig. S4 shows the XPS peak deconvolution for O 1s spectra of biochar samples. The peak of 531.75 eV was assigned to O—H bonds. The peak of 532.95 and 533.50 eV were ascribed to O—C and C═O bonds, respectively. From the O 1s spectra of biochar, it was clearly found that the oxygen amount of modified biochar was higher than unmodified biochar. As can be seen from Figs. 4 and S4, the amount of surface contained oxygen functional groups of modified biochar are significantly higher than unmodified biochar, which can be reflected by the direct comparison of C 1s spectra between biochars and modified biochar samples. These peak area rations of C═C, C—C, C—OH, C—O—C and —COOH bonds are evaluated in Table 2. The number of C═C components increased from 72.08% to 74.40%. The amount of C—OH increased from 6.20% to 6.49%. Notably, the amount of C—O—C and —COOH increased after one-step modification process. The amount of C═C, C—OH, C—O—C and —COOH components was higher than that of unmodified biochar, which confirmed that one-step modification process increased the amount of functional groups. Therefore, the content of carbon and oxygen of modified biochar increased (Table 1) due to the oxygen-containing functional groups increase. However, the abundance of oxygen-containing functional groups decreased slightly with increasing pyrolysis temperature from 300 to 700 °C. Thus, the carbon and oxygen of modified biochar decreased slightly as increasing pyrolysis temperature. This results was consistent with the findings of Xue et al. (2012) study. Their research exhibited that the carbon was oxidized by H_2O_2 activation, which resulted in an increased number of contained oxygen functional groups. Notably, the one-step synthesis has resulted in obvious larger SSA and more functional groups than pristine biochar, which may facilitate the adsorption of EDCs and heavy metals from water.

Fig. S5 displays the deconvoluted XPS spectra for different Fe species on the surface of biochar samples. The double peaks of 712.0 and 724.1 eV were characteristic of Fe $2p_{3/2}$ and Fe $2p_{1/2}$, respectively (Zhu et al., 2014). Two peaks of 710.9 and 713.2 eV, which were classified to Fe^{3+} and Fe^{2+}, indicated the presence of magnetite (Fe_3O_4) in the materials. Two other peaks at 724.0 and 725.8 eV were assigned to the hematite and maghemite portions, respectively. It was seen on the XPS spectra of the AMBCs (Grosvenor et al., 2004).

3.2. Single–solute adsorption

3.2.1. Adsorption kinetics

The adsorption kinetics of E2 and Cu(II) onto biochar materials are presented in Fig. 5. At same E2 concentration, the adsorption capacity of biochars were 83.20, 93.74, 95.40, 100.80, 107.20 and 116.70 mg/g for RBC, MBC, ABC, AMBC-300, AMBC-500 and AMBC-700 respectively.

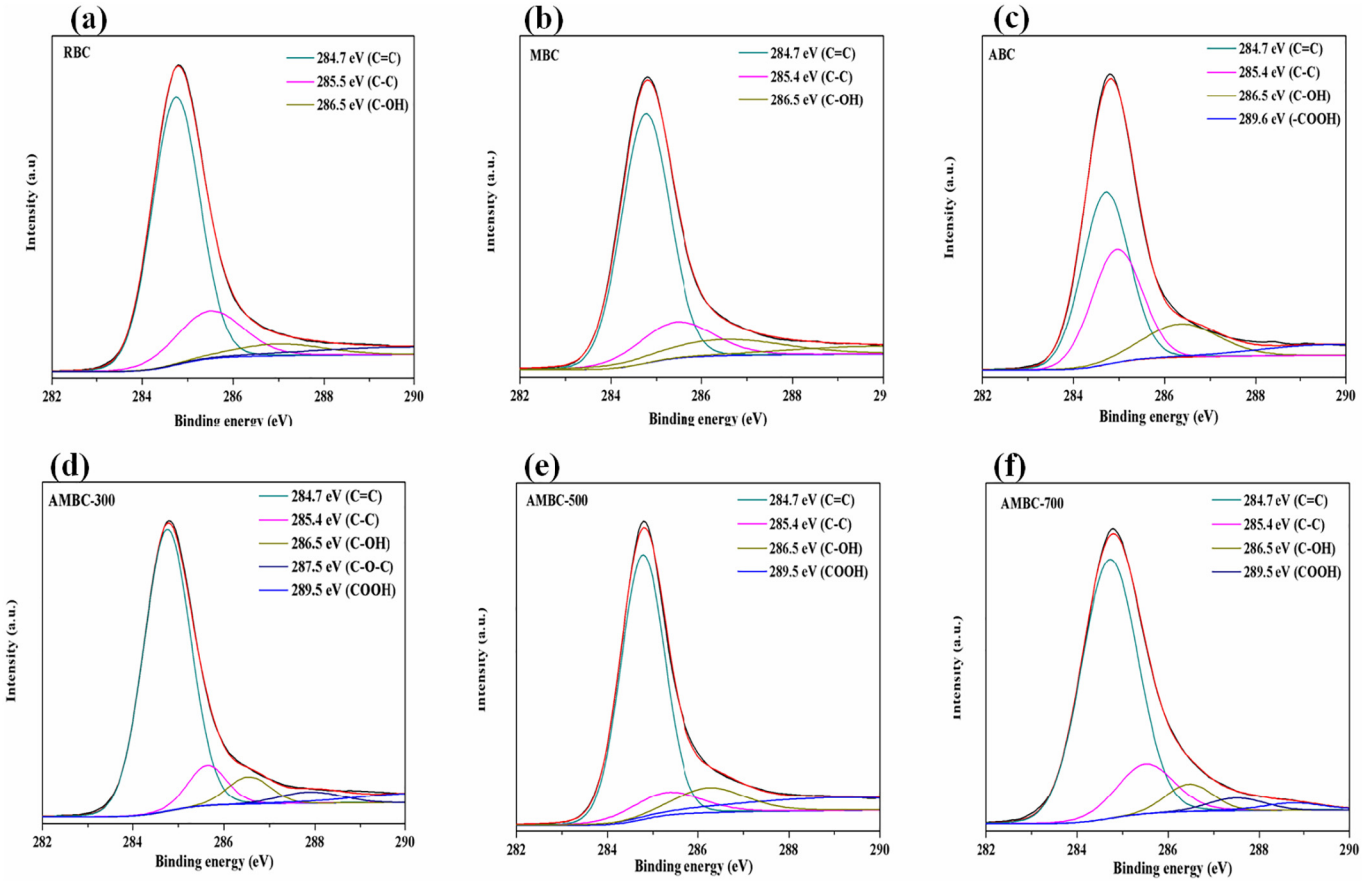

Fig. 4. XPS spectra of C 1s for RBC (a), MBC (b), ABC (c), AMBC-300 (d), AMBC-500 (e) and AMBC-700 (f).

The adsorption capacity of AMBC-700 for E2 was 1.4 times than RBC. The adsorbed amount of modified biochars was much larger than that of unmodified biochar, and the adsorption capacity increased with increasing in the pyrolysis temperature. However, the quality adsorbed of Cu(II) were 38.21, 50.30, 58.10, 74.12, 64.72 and 60.31 mg/g for RBC, MBC, ABC, AMBC-300, AMBC-500 and AMBC-700, respectively. The adsorption efficiency of modified biochar was much higher than that of unmodified biochar. According to the above result, 400 and 600 min were chose for contact time of the adsorption equilibrium in further E2 and Cu(II) adsorption studies, respectively.

In order to further analyze the adsorption process of biochar samples, two kinetic models (pseudo-first-order and pseudo-second-order) were used to fit the experiment data. The two nonlinear kinetics models are illustrated in Table. S2. The kinetics parameters calculated from two models are listed in Table S3. Analysis of kinetics parameters, the value of determination coefficients in pseudo-second-order model was much higher than that of pseudo-first-order model for E2 adsorption process. For Cu(II) adsorption process, the correlation coefficient (R^2) suggested that the pseudo-second-order model was better fitted with the experiment results than pseudo-first-order model. Therefore, both the kinetics of E2 and Cu(II) adsorption could be well described by pseudo-second-order. This indicated that the adsorption process of both E2 and Cu(II) was chemisorption process (Jiang et al., 2016).

Table 2
The peak area ratio of C═C, C—C, C—OH, C—O—C, and —COOH bonds to the C 1s XPS spectra of biochar samples.

Binding energy (eV)	284.7 eV	285.5 eV	286.5 eV	287.5 eV	289.5 eV
Functional group	C═C (%)	C—C (%)	C—OH (%)	C—O—C (%)	—COOH (%)
RBC	72.08	19.15	6.20	≈0	≈0
MBC	70.07	16.78	6.14	≈0	≈0
ABC	65.40	16.29	6.30	4.82	≈0
AMBC-300	74.40	10.51	6.49	5.59	7.40
AMBC-500	73.35	9.58	6.46	5.31	6.12
AMBC-700	72.32	9.20	6.36	4.85	5.14

Intra-particle diffusion model was further examined due to above kinetics model were not able to analyze the diffusion mechanism. The equation for intra-particle diffusion is shown in Table S2. Based on the model, if the value of C_i was zero, indicating that the adsorption rate is controlled by intra-particle diffusion for the all adsorption stage (Wu et al., 2014). For a solid/liquid sorption process, the adsorption process may include third steps: external mass transfer (film diffusion), intra-particle diffusion and adsorption on the internal surface of the adsorbent. Based on these plots of intraparticle diffusion, both the sorption process of E2 and Cu(II) are comprised by three phases. The first sharper slope may be due to the film diffusion, the second parts were the intraparticle diffusion on AMBCs, and last portions meant equilibrium stages, which might due to the diffusion became to stable as less number of available sorption sites of adsorbents or low E2 and Cu(II) concentration in the aqueous system. Therefore, both the adsorption of E2 and Cu(II) by AMBCs might include both surface sorption and intraparticle diffusion mechanisms. The model parameters obtained from the model are listed in Table S4. For both E2 and Cu(II), the all values of C_i are not zero, which indicated that intra-particle diffusion was present as a part of diffusion process while it was not the rate-controlling step in all the process.

3.2.2. Adsorption isotherm

The adsorption isotherms of E2 and Cu(II) onto RBC, MBC, ABC, AMBC-300, AMBC-500 and AMBC-700 are shown in Fig. 6. It can be seen that the uptake rapidly increased in the initial stage and then slowly increased until the adsorption reached equilibrium. The rapid

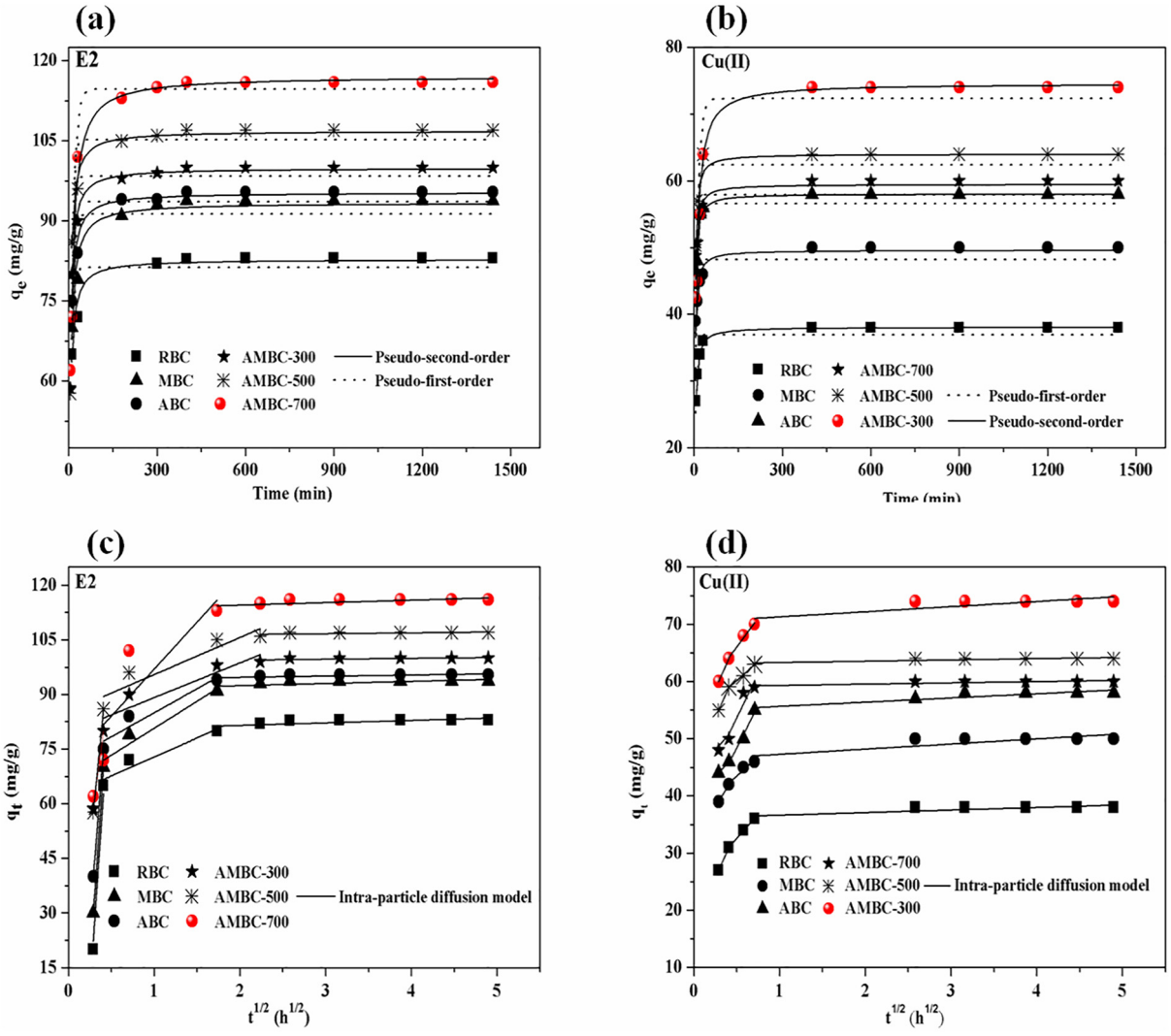

Fig. 5. Pseudo-first-model and pseudo-second-model for E2 adsorption (a). Pseudo-first-model and pseudo-second-model for Cu(II) adsorption (b), Intra-particle diffusion model for E2 adsorption (c), Intra-particle diffusion model for Cu(II) adsorption (d).

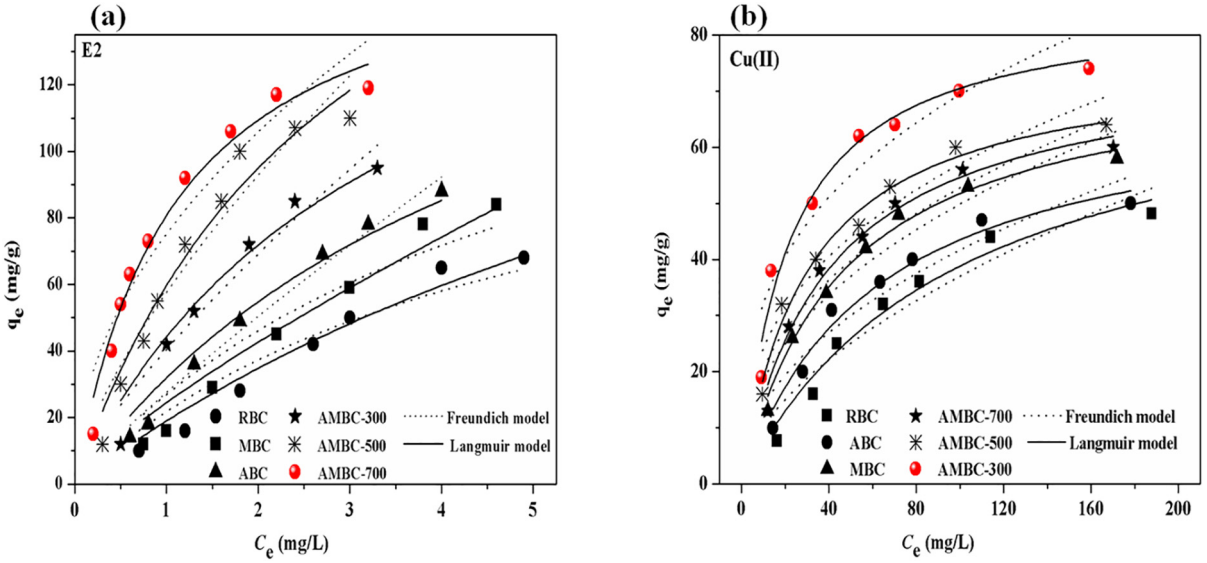

Fig. 6. Adsorption isotherm of E2 (a) and Cu(II) (b) by RBC, MBC, ABC, AMBC-300, AMBC-500, and AMBC-700.

increase of removal efficiency in the initial stages probably because of the sorbent has plenty of readily accessible active sites on the surface of biochar (Jiang et al., 2016). However, the adsorption rate became slowly, which might be caused by the decrease of active sites with adsorption time (Ramesha et al., 2011). Similar phenomenon was also observed by Jiang et al. (2016) study. The adsorption isotherms models can provide more insights into the adsorption characteristics. Therefore, the nonlinear fit of the isotherm model of Langmuir and Freundich are shown in Fig. 6. Nonlinear forms of the isotherm models of Langmuir and Freundich are shown in Table. S5. The Langmuir model assumes that the adsorption of pollutants occurs as monolayers on a homogeneous surface of an adsorbent (Hu et al., 2011) while Freundich model assumes that structurally heterogeneous mechanism and not restricted to the formation of the monolayer (Li et al., 2017a). Adsorption parameters in the equilibrium aqueous concentration range were calculated according to the isotherm fitting and are listed in Tables 3 and S6. Furthermore, two parameters including the root mean square error (*RMSE*) and chi-square test (χ^2) values were calculated. As shown in Table 3, both in E2 and Cu(II) adsorption process, the Langmuir model shows the highest R^2 and the lowest error functions values than Freundich model, indicating that adsorption process of E2 and Cu(II) were monolayers on a homogeneous surface of biochar.

The maximum adsorption capacity (q_{max}) for E2 adsorption were 89.25, 103.20, 110.30, 125.30, 140.12 and 153.20 mg/g for RBC, MBC, ABC, AMBC-300, AMBC-500 and AMBC-700, respectively. The maximum adsorption capacity of E2 was achieved for AMBC-700 (153.20 mg/g) calculated from Langmuir model. The adsorption capacity of AMBC-700 (153.20 mg/g) was approximately 1.71 times than of RBC (89.25 mg/g). The trend correlated with that of the SSA. The SSA of AMBC-700 was the largest among modification biochars, which provided more adsorption sites and thus resulted the adsorption capacity larger than unmodified biochar (Wang et al., 2014). Thus, the SSA played a critical role in the E2 adsorption process. In a word, the adsorption capacity of modified biochar, especially for AMBC-700, was significantly increased compare to pristine biochar.

For Cu(II), the Langmuir model descried the metal adsorption better than the Freundlich model, indicating a maximum metal sorption capacity at high metal concentration. These results were consistent with the concept of metals interacting with a limited number of specific sorption sites (B. Han et al., 2015). The maximum Cu(II) q_{max} (mg/g) obtained from Langmuir model were 85.93, 80.33, 79.39, 75.25, 70.59 and 65.40 mg/g for AMBC-300, AMBC-500, AMBC-700, ABC, MBC and RBC, respectively, indicating that the activation and magnetization enhanced adsorption capacity of Cu(II). Furthermore, comparing with RBC, the AMBC-700, AMBC-500, especially AMBC-300 showed highest adsorption capacity for Cu(II). It could be ascribed to their higher surface area, larger pore size and abundant functional groups, which provided more active adsorption sites for Cu(II) adsorption. According to the results from Table 1, the SSA of AMBC-700 was the largest among modification biochars, but the adsorption capacity of Cu(II) did not show the maximum adsorption. This indicated that the sorption ability was not complete controlled by SSA, other reason such as contained oxygen functional groups may contribute to the Cu(II) sorption. Sorption of heavy metal ion from water is generally governed by surface chemistry and surface area of the sorbent or complexation. The surface complexation between metals and functional groups of biochars was an important mechanism in sorption process (J. Sun et al., 2014). Biochar might be involved in coordination with Cu(II) due to surface complexation with carboxyl or hydroxyl functional groups. The complexation between —COOH/—OH functional groups of biochars and metal ions usually promote their sorption due to the oxygen-containing functional groups could provide sites for metal ions sorption (Cao et al., 2009). The number of contained oxygen functional groups of AMBC-300 was the highest among modified biochars (confirmed by XPS and Table 2). Therefore, AMBC-300 showed highest adsorption capacity for Cu(II), which indicated that the amount of contained oxygen functional groups also played an important role except for SSA in the adsorption process of Cu(II).

Table 3
Parameters of Langmuir model for E2 and Cu(II) adsorption.

Adsorbents	Pollutants	Langmuir				
		q_{max} (mg/g)	K_L (L/mg)	R^2	*RMSE*	χ^2
RBC	E2	89.25	0.37	0.96	2.83	13.32
	Cu(II)	65.40	0.02	0.96	2.81	17.88
MBC	E2	103.20	0.20	0.97	5.23	43.22
	Cu(II)	70.59	0.02	0.98	2.53	16.42
ABC	E2	110.30	0.10	0.98	4.64	21.55
	Cu(II)	75.25	0.01	0.98	1.70	12.89
AMBC-300	E2	125.30	0.11	0.97	5.22	27.27
	Cu(II)	85.93	0.02	0.98	2.59	16.71
AMBC-500	E2	140.12	0.21	0.98	4.31	18.54
	Cu(II)	80.33	0.03	0.98	2.31	15.32
AMBC-700	E2	153.20	0.73	0.98	4.83	23.32
	Cu(II)	79.39	0.05	0.98	3.77	14.22

3.2.3. Effects of pH on adsorption process

Fig. 7a shows the effect of initial pH on E2 adsorption by RBC, MBC, ABC, AMBC-300, AMBC-500, and AMBC-700 with pH range from 2.0 to 11.0, respectively. As seen, the adsorption capacities of biochar samples decreased when pH range from 2.0 to 3.0, then increased when pH range from 3.0 to 7.0. Further increasing in pH from 7.0 to 11.0 caused significant reduction of the sorption. These phenomena might be caused by the change of the surface charge of biochars and the E2 speciation at different pH. The pH_{zpc} of all biochar materials was found to be 3.25–6.26 (Table 1). When $pH < pH_{zpc}$, the zeta potential values was found to be positive, which was likely caused by the surface coverage with maghemite (mainly $FeOH_2^+$). E2 might become protonated at pH was 2.0 due to hydroxyl or ketonic groups (Ahmed et al., 2018), resulting in a positive charge. Hence, the electrostatic repulsion might cause lower adsorption capacity. Increase in pH from 3.0 to 7.0 increased the sorption capacity, which might be due to the formation of strong hydrogen bonds together with electron donor-acceptor (EDA) interactions. In addition, when $pH > pH_{zpc}$, the zeta potential values was found to be negative. Hence, the electrostatic attraction might cause higher sorption. Further pH increases up to 11.0, it caused a decrease of adsorption capacity for E2. It has been reported that the pK_a of E2 is 10.4 (Lee et al., 2005). The microspecies distribution (Jiang et al., 2017) of E2 molecule in aqueous is shown in Fig. S6. When pH is around 10.0, E2 would start deprotonating, resulting in a negative charge. The low adsorption capacity of biochar at this pH might be explained that the highly electrostatic repulsion between the negatively charged biochar and the E2 anion. Additionally, deprotonation would break the hydrogen bonds between biochar and E2 though replacement with the protons on E2 molecules. EDA interactions and hydrogen bond were not strong as solution pH was above the p*K*a values of E2 (Ahmed et al., 2018). Therefore, the alkaline conditions lead to low adsorptive capacity of biochars. The results exhibits that acidic conditions is conducive to the adsorption of E2, which is consistent with the results of Jiang et al. (2016).

The results of adsorption of Cu(II) by biochars at different pH was presented in Fig. 7b. $Cu(OH)^{2+}$ was formed in the pH range from 6.6 to 11. Therefore, the experiments were conducted for Cu(II) adsorption with pH range from 2.0 to 6.0 due to avoid precipitation of $Cu(OH)^{2+}$. It could be clearly seen that the adsorption ability for Cu(II) was increased slight when increasing the pH and the highest adsorption capacity was observed at pH around 5.0. The phenomenon might explained that the pH_{zpc} of materials. When the solution $pH < pH_{zpc}$, the surface of biochars was positively charged, indicating that heavy metal adsorption was favored at high pH because the high concentrations of H_3O^+ at lower pH caused effective competitive with metal ions for adsorption sites (Zhou et al., 2018).

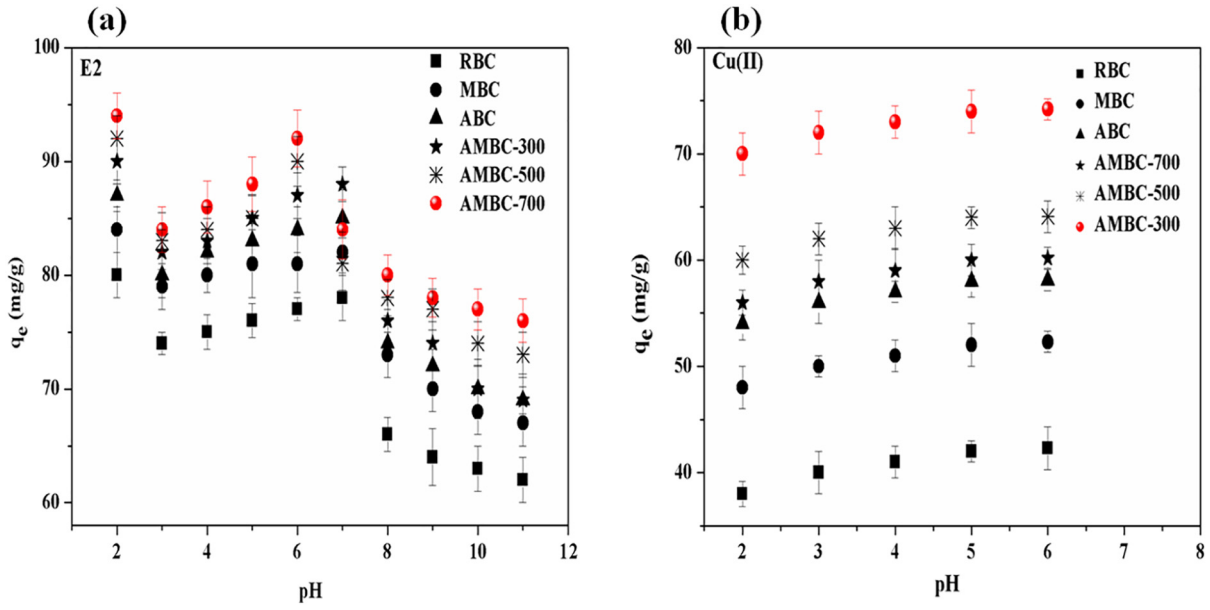

Fig. 7. Effect of initial solution pH value on adsorption process of E2 (a) and Cu(II) (b) for RBC, MBC, ABC, AMBC-300, AMBC-500, and AMBC-700.

3.3. Binary–solute adsorption

Sorption of Cu(II) and E2 on biochars may have similar adsorption process according to the results of kinetics and isotherms. There may exist the adsorption site competition between Cu and E2. Consequently, it is necessary to investigate the adsorption of Cu(II) and E2 in binary-solute system.

To evaluate the influence of the simultaneous existence of E2 and Cu (II) on their mutual adsorption onto biochar, the adsorption experiment in binary-solute system were carried by varying E2/Cu(II) concentration with another one fixed, and the results are shown in Fig. 8. From Fig. 8a, under the same initial Cu(II) concentration, the adsorption capacity for E2 were in the following order: AMBC-700 > AMBC-500 > AMBC-300 > ABC > MBC > RBC. The q_e (mg/g) values of AMBC-700 for E2 were when Cu(II) concentration increase from 0 to 60 mg/L: 116, 120, 123, 108, 100, 95 and 90 mg/g, respectively. It could clearly indicated that the presence of low Cu(II) concentration (10 and 20 mg/L) can enhance the E2 adsorption compare to the single E2 adsorption, which might be attributed to the formed biochars-E2-Cu(II) or biochars-Cu(II)-E2 complexes. Furthermore, when increased the coexisting Cu(II) concentration from 20 to 60 mg/L, the adsorption capacity of E2 decreased, which indicated that the complexes interact between Cu(II) and E2 occurred only the presence of low Cu(II) concentration and small portion, and greater competitive adsorption between them on biochar at higher Cu(II) concentration. The effects of coexisting E2 on Cu(II) adsorption onto biochar samples were also measured. As seen in Fig. 8b, the q_e (mg/g) values of AMBC-300 for Cu(II) under different E2 concentration (from 0 to 6 mg/L) were 74, 75, 76, 70, 65, 58 and 57 mg/g, respectively. It could be clearly observed that the adsorption capacity of Cu(II) increased slight as the initial E2 concentration and decreased by 26% when E2 concentration range from 3 to 6 mg/L. The results were similar to Zhou et al. (2017) results that the presence of high Cu(II) concentration would decrease the adsorption of tetracycline (Chen et al., 2007). It have been reported that addition of Cu(II) decreased sorption of

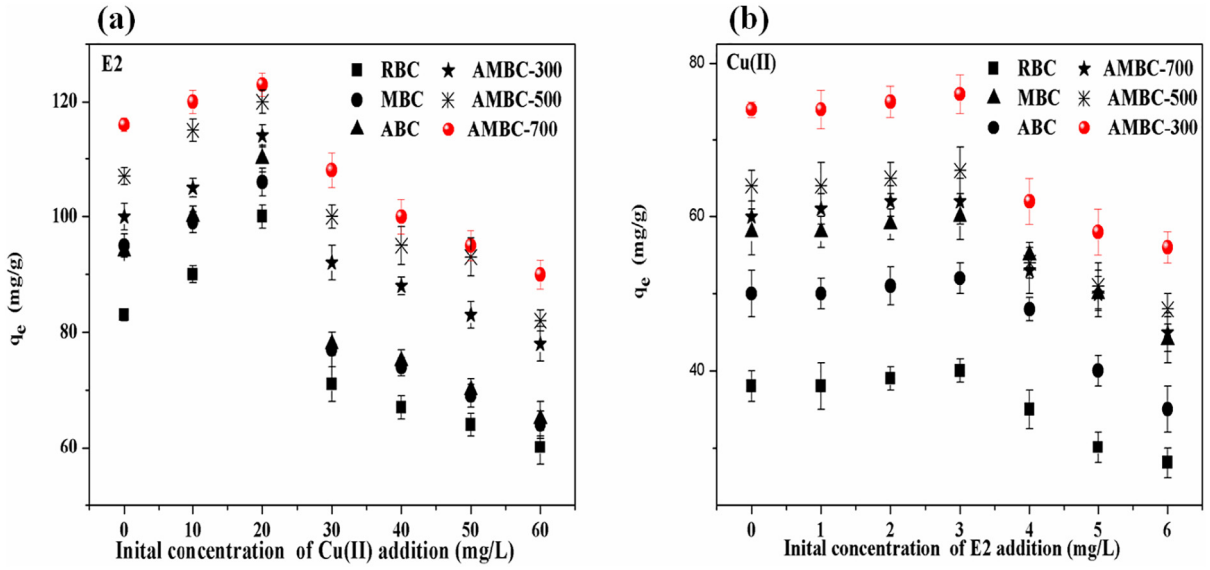

Fig. 8. The E2 (6 mg/L) adsorption with Cu(II) addition (0–60 mg/L) (a) and the Cu(II) (140 mg/L) adsorption with E2 addition (1–6 mg/L) (b).

naphthalene, 2,4-dichlorophenol, 1,2-dichlorobenzene by 30–60%. They assumed that the surface complexation of Cu(II) to form, which directly competed with organics for surface adsorption active sites. As previous discussion, E2 and Cu(II) might be sorbed by functional groups and porous structure of adsorbent. Therefore, it could be deduced that the E2 and Cu(II) had some same sorption sites, which consequently resulted in competition adsorption between E2 and Cu(II). Competition for the same surface sites likely reduced their individual sorption capacities. The q_e (mg/g) values of E2 and Cu(II) decreased by 20.70% and 22.90% in binary-solute system, respectively. Results showed that the low E2 and Cu(II) concentration would enhance their adsorption onto biochars. By comparison with single adsorption system, new adsorption pathways could exist in binary-solute system. The Cu(II) could act as a bridge between the biochar and E2, which resulted in the formation of biochar-Cu(II)-E2 or biochar-E2-Cu(II). Therefore, the adsorption capacity of E2 and Cu(II) increased at their low concentration. However, the great competition between them at high concentration suppressed both of their sorption, which could be due to competing active adsorption sites.

3.4. Adsorption mechanism

The adsorption mechanism for E2 and Cu(II) adsorption onto AMBCs were determined according to the above results analysis. For detailed studies, AMBC-700 and AMBC-300 were selected due to their highest adsorption capacity for E2 and Cu(II) among biochar materials. The pseudo-second-order could fit the experiment data well, indicating that the surface functional groups played an important role in the E2 adsorption process (Ahmed et al., 2018). It could be conclude that the sorption process of E2 involve chemisorption and rate-limit step. E2, with the several fused aromatic rings, is π electron-rich. Meanwhile, AMBC-700 consisted of carboxylic —C═O functional groups (as confirmed by XPS and FTIR), which might act as π-electron acceptor site for the interactions and the —OH in E2 could act as π-electron donor site. This abundant π electron-rich can easily form stronger EDA interactions. In order to studied the molecular interaction of E2 with AMBC-700, the FTIR spectra of AMBC-700 after E2 adsorption (AMBC-700-E2) is shown in Fig. 2c. The peak of 1607 cm^{-1} (C═C) shifted from 1607 cm^{-1} to 1626 cm^{-1} after E2 adsorption, which confirmed that the formation of π-π interactions. In addition, the peaks corresponding to the skeletal vibration of O—H also shifted from 3435 to 3387 cm^{-1}, indicating strong associating O—H was formed after adsorption of E2, and the peaks of 1029 cm^{-1} (C—O) shifted from 1029 to 1090 cm^{-1}. The changes indicated the formation of hydrogen bonds between the oxygen-containing functional groups of AMBC-700 and E2 molecules. The results indicated that the E2 was adsorbed by hydrogen bonds, π-π EDA interactions and electrostatic attraction.

For Cu(II), the FTIR spectra of AMBC-300 after Cu(II) adsorption (AMBC-300-Cu(II)) is shown in Fig. 2c. FTIR shows reduction of the bands at 1514 cm^{-1} and 1265 cm^{-1}, attributing to the lignin C═C stretching and the phenolic —OH stretching vibration, respectively. As reported, the aromatic structure of biochar could act as π donors and the functional groups of adsorbent were essential for metal removal because they could interact with heavy metal by metal-π interactions (Harvey et al., 2011). Fang et al. (2014) reported that biochar contain many functional groups such as —COOH, C—O, which could interact with metal to form complexes. Therefore, the possible mechanisms could be exhibited schematically as follows:

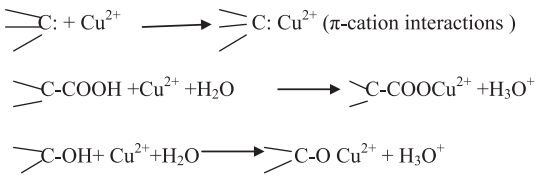

Furthermore, the intense peak at 3396 cm^{-1} confirmed the formation of $Cu(OH)_2$. This could be suggested that Cu(II) sorption by AMBC-300 was probably through a surface sorption mechanism via coordination of Cu(II) d-electron to C═C (π-electrons) bond and —O—Cu bond. Complexation of metals with ionized O-containing groups (e.g. —COOH and —O—) or C═C (π-electrons) bond has been proposed to be the major mechanism for heavy metal sorption (Swiatkowski et al., 2004). The amount of —COOH, C—OH, C═O components of AMBC-300 are large than that of other biochars (Table 2). This might be explained that the greater enhancement of the specific adsorption of Cu (II) by AMBC-300. This finding was likely the reason why the adsorption capacity was decreased in the binary-solute system due to the competitive contained oxygen functional groups (e.g —COOH or —OH).

3.5. Cycles and comparison

A good adsorbent should have high adsorption capacity as well as effective reusability. Thus, the adsorption performance of the regenerated AMBC-700 and AMBC-300 is exhibited in Fig. S7. As seen, the adsorption capacity of regenerated biochar gradually decreased. The adsorption ability of AMBC-700 and AMBC-300 decreased only by approximately 13.79% and 12.16% after fifth cycles, respectively, compared with that of the first cycle. This could be explained by the loss of surface functional groups after each desorption process. The experimental results demonstrated that the adsorbent not only could be easily separated, but its regeneration efficiency was relatively high. Therefore, the one-step modified biochar could be used as adsorbent in practice application.

The q_{max} values of modified biochar for E2 and Cu(II) were 153.20, 85.93 mg/g, respectively. Compared with the RBC, the adsorption capacity (q_m) of AMBC-700 and AMBC-300 increased 71.0% and 31.4% for E2 and Cu(II), respectively. These results are comparable to other reported adsorbents shown in Table 4. As seen, the adsorption capacity of AMBC-700 and AMBC-300 for E2 and Cu(II) was relatively higher than some

Table 4
Comparison of Cu(II) and E2 removal adsorption capacity in this study with other adsorbents.

Adsorbents	BET surface area (m^2/g)	Quantity adsorbed (mg/g)	Experiment conditions			References
			pH	C_0 (mg/L)	m(adsorbent) (mg)	
DBC-PM	8.61	43.68 (Cu(II))	–	50	250	(Batool et al., 2017)
DBC-FYM	10.11	45.50 (Cu(II))	–	50	250	(Batool et al., 2017)
CPMB	–	71.40 (Cu(II))	5.00	100		(Deng et al., 2017)
PM350	636.00	30.00 (Cu(II))	5.00	10		(Peng et al., 2017)
FMBC	71.64	64.90 (Cu(II))		50	1000	(Zhou et al., 2018)
SABC	2.36	48.49 (Cu(II))	–	50	2	(M. Li et al., 2013; Y. Li et al., 2013)
AMBC-300	263.21	85.93 (Cu(II))	5.00	140	40	This study
Few-layered graphene oxide nanosheets	92.00	149.40 (E2)	7.00	3	3	(Jiang et al., 2016)
CGMC	298.90	85.80 (E2)	7.00	2	5	(Jiang et al., 2017)
Multi-walled carbon nanotubes	–	27.20 (E2)	–	2.4	5	(Sun and Zhou, 2014)
Hydrochar-FMBO	167.17	49.77 (E2)	7.00	6	5	(Ning et al., 2017)
AMBC-700	357.84	153.20 (E2)	5.00	6	5	This study

previous studies reported, respectively. Such comparison showed that AMBCs by one-step synthesis method was an efficient adsorbent in treatment E2 and Cu(II) wastewater.

4. Conclusions

This work studied that AMBCs were successfully synthesized via one-step synthetic method with different temperature (300, 500 and 700 °C) for the removal of E2 and Cu(II) in single/binary-solute system. The magnetization process made biochar more easier separation from aqueous media. The activation process improved significantly SSA, and contained oxygen functional groups compared to pristine biochar, which further increased the adsorption capacity for E2 and Cu(II). The maximum adsorption capacity (q_{max}) obtained from Langmuir model of E2 onto AMBC-700 and Cu(II) onto AMBC-300 were 153.20, 85.93 mg/g, respectively. The initial pH of the solution influenced the adsorption of E2 and Cu(II). Coexisted Cu(II) and E2 at their low concentration enhanced the adsorption by the complexing bridging mechanism in the binary-solute system. The adsorption capacity was decreased at their high concentration due to the competitive adsorption sites. In term of sorption mechanism, E2 sorption mainly occurred through π-π EDA interactions and by forming hydrogen bonds. Cu(II) mainly adsorption by the complexes of Cu(II) and oxygen-containing functional groups. Therefore, the AMBCs by one-step synthesis could be used as an effective adsorbent for removing simultaneously EDCs and heavy metal from water.

Acknowledgements

This research was financially supported from the National Natural Science Foundation of China (Grant No. 51609268), the Key Project of Technological Innovation in the Field of Social Development of Hunan Province, China (Grant Nos. 2016SK2010 and 2016SK2001), the Fundamental Research Funds for the Gentral Universities, and the Natural Science Foundation of Hunan Province, China (Grant Nos. 2018JJ3040 and 2018JJ3096).

Appendix A. Supplementary data

Supplementary data to this article can be found online at https://doi.org/10.1016/j.scitotenv.2018.05.130.

References

Ahmed, M.B., Zhou, J.L., Ngo, H.H., Johir, M.A.H., Sornalingam, K., 2018. Sorptive removal of phenolic endocrine disruptors by functionalized biochar: competitive interaction mechanism, removal efficacy and application in wastewater. Chem. Eng. J. 335, 801–811.

Akhavan, O., Ghaderi, E., Emamy, H., Akhavan, F., 2013. Genotoxicity of graphene nanoribbons in human mesenchymal stem cells. Carbon 54, 419–431.

Angin, D., Altintig, E., Kose, T.E., 2013. Influence of process parameters on the surface and chemical properties of activated carbon obtained from biochar by chemical activation. Bioresour. Technol. 148, 542–549.

Atkinson, S.K., Marlatt, V.L., Kimpe, L.E., Lean, D.R.S., Trudeau, V.L., Blais, J.M., 2011. Environmental factors affecting ultraviolet photodegradation rates and estrogenicity of estrone and ethinylestradiol in natural waters. Arch. Environ. Contam. Toxicol. 60, 1–7.

Bastami, T.R., Entezari, M.H., 2012. Activated carbon from carrot dross combined with magnetite nanoparticles for the efficient removal of p-nitrophenol from aqueous solution. Chem. Eng. J. 210, 510–519.

Batool, S., Idrees, M., Hussain, Q., Kong, J., 2017. Adsorption of copper (II) by using derived-farmyard and poultry manure biochars: efficiency and mechanism. Chem. Phys. Lett. 689, 190–198.

Bradley, P.M., Writer, J.H., 2014. Effect of light on biodegradation of estrone, 17β-estradiol, and 17α-ethinylestradiol in stream sediment. J. Am. Water. Resour. Assoc. 50, 334–342.

Cao, X., Ma, L., Gao, B., Harris, W., 2009. Dairy manure derived biochar effectively sorbs lead and atrazine. Environ. Sci. Technol. 43, 3285–3291.

Cazetta, A.L., Pezoti, O., Bedin, K.C., Silva, T.L., Paesano Junior, A., Asefa, T., Almeida, V.C., 2016. Magnetic activated carbon derived from biomass waste by concurrent synthesis: efficient adsorbent for toxic dyes. ACS Sustain. Chem. Eng. 4, 1058–1068.

Chen, J., Zhu, D., Sun, C., 2007. Effect of heavy metals on the sorption of hydrophobic organic compounds to wood charcoal. Environ. Sci. Technol. 41, 2536–2541.

Chen, D., Chen, X., Sun, J., Zheng, Z., Fu, K., 2016. Pyrolysis polygeneration of pine nut shell: quality of pyrolysis products and study on the preparation of activated carbon from biochar. Bioresour. Technol. 216, 629–636.

Deng, J., Liu, Y., Liu, S., Zeng, G., Tan, X., Huang, B., 2017. Competitive adsorption of Pb(II), Cd(II) and Cu(II) onto chitosan-pyromellitic dianhydride modified biochar. J. Colloid Interface Sci. 506, 355–364.

Fan, Z., Hu, J., An, W., Yang, M., 2013. Detection and occurrence of chlorinated byproducts of bisphenol A, nonylphenol, and estrogens in drinking water of China: comparison to the parent compounds. Environ. Sci. Technol. 47, 10841–10850.

Fang, Q., Chen, B., Lin, Y., Guan, Y., 2014. Aromatic and hydrophobic surfaces of wood-derived biochar enhance perchlorate adsorption via hydrogen bonding to oxygen-containing organic groups. Environ. Sci. Technol. 48, 279–288.

Gollavelli, G., Chang, C.C., Ling, Y.C., 2013. Facile synthesis of smart magnetic graphene for safe drinking water: heavy metal removal and disinfection control. ACS Sustain. Chem. Eng. 1, 462–472.

Grosvenor, A.P., Kobe, B.A., Biesinger, M.C., McIntyre, N.S., 2004. Investigation of multiplet splitting of Fe 2p XPS spectra and bonding in iron compounds. Surf. Interface Anal. 36, 1564–1574.

Han, Z., Sani, B., Mrozik, W., Obst, M., Beckingham, B., Karapanagioti, H.K., Werner, D., 2015. Magnetite impregnation effects on the sorbent properties of activated carbons and biochars. Water Res. 70, 394–403.

Han, B., Zhang, M., Zhao, D.Y., Feng, Y.C., 2015. Degradation of aqueous and soil-sorbed estradiol using a new class of stabilized manganese oxide nanoparticles. Water Res. 70, 288–299.

Harvey, O.R., Herbert, B.E., Rhue, R.D., Kuo, L.J., 2011. Metal interactions at the biochar-water interface: energetics and structure-sorption relationships elucidated by flow adsorption microcalorimetry. Environ. Sci. Technol. 45, 5550–5556.

Hu, X.J., Wang, J.S., Liu, Y.G., Li, X., Zeng, G.M., Bao, Z.L., Zeng, X., Chen, A.W., Long, F., 2011. Adsorption of chromium (VI) by ethylenediamine-modified cross-linked magnetic chitosan resin: isotherms, kinetics and thermodynamics. J. Hazard. Mater. 185, 306–314.

Jiang, L.H., Liu, Y.G., Zeng, G.M., Xiao, F.Y., Hu, X.J., Hu, X., Wang, H., Li, T.T., Zhou, L., Tan, X.F., 2016. Removal of 17β-estradiol by few-layered graphene oxide nanosheets from aqueous solutions: external influence and adsorption mechanism. Chem. Eng. J. 284, 93–102.

Jiang, L.H., Liu, Y.G., Liu, S.B., Hu, X.J., Zeng, G.M., Hu, X.J., Liu, S.M., Liu, S.H., Huang, B.Y., Li, M.F., 2017. Fabrication of β-cyclodextrin/poly (ι-glutamic acid) supported magnetic graphene oxide and its adsorption behavior for 17β-estradiol. Chem. Eng. J. 308, 597–605.

Johnson, A.C., Dumont, E., Williams, R.J., Oldenkamp, R., Cisowska, I., Sumpter, J.P., 2013. Do concentrations of ethinylestradiol, estradiol, and diclofenac in European rivers exceed proposed EU environmental quality standards. Environ. Sci. Technol. 47, 12297–12304.

Jung, K., Choi, B., Jeong, T., Ahn, K., 2016. Facile synthesis of magnetic biochar/Fe_3O_4 nanocomposites using electro-magnetization technique and its application on the removal of acid orange 7 from aqueous media. Bioresour. Technol. 672–676.

Lee, Y., Yoon, J., Cunten, U., 2005. Supporting information for kinetics of the oxidation of phenols and phenolic endocrine disruptpors during water treatment with ferrate (Fe(VI)). Environ. Sci. Technol. 39, 8978.

Li, M., Liu, Q., Guo, L., Zhang, Y., Lou, Z., Wang, Y., 2013. Cu(II) removal from aqueous solution by *Spartina alterniflora* derived biochar. Bioresour. Technol. 141, 83–88.

Li, Y., Zhu, C.L., Lu, T., Guo, Z.P., Zhang, D., Ma, J., Zhu, S.M., 2013. Simple fabrication of a Fe_2O_3/carbon composite for use in a high-performance lithium ion battery. Carbon 52, 565–573.

Li, M.F., Liu, Y.G., Liu, S.B., Shu, D., Zeng, G.M., Hu, X.J., Tan, X.F., Jiang, L.H., Yan, Z.L., Cai, X.X., 2017a. Cu(II)-influenced adsorption of ciprofloxacin from aqueous solutions by magnetic graphene oxide/nitrilotriacetic acid nanocomposite: competition and enhancement mechanisms. Chem. Eng. J. 319, 219–228.

Li, M.F., Liu, Y.G., Zeng, G.M., Liu, S.B., Hu, X.J., Shu, D., Jiang, L.H., Tan, X.F., Cai, X.X., Yan, Z.L., 2017b. Tetracycline absorbed onto nitrilotriacetic acid-functionalized magnetic graphene oxide: influencing factors and uptake mechanism. J. Colloid Interface Sci. 269–279.

Lua, A.C., Yang, T., 2004. Effects of vacuum pyrolysis conditions on the characteristics of activated carbons derived from pistachio-nut shells. J. Colloid Interface Sci. 276, 364–372.

Lucas, I.T., Vidal, S.D., Dubis, E., Chevalet, J., Turq, P., 2007. Surface charge density of maghemite nanoparticles: role of electrostatics in the proton exchange. J. Phys. Chem. C 111, 18568–18576.

Manya, J.J., 2012. Pyrolysis for biochar purposes: a review to establish current knowledge gaps and research needs. Environ. Sci. Technol. 46, 7939–7954.

Mohan, D., Sarswat, A., Singh, V.K., Alexandre Franco, M., Pittman, C.U., 2011. Development of magnetic activated carbon from almond shells for trinitrophenol removal from water. Chem. Eng. J. 172, 1111–1125.

Nethaji, S., Sivasamy, A., Mandal, A.B., 2013. Preparation and characterization of corn cob activated carbon coated with nano-sized magnetite particles for the removal of Cr (VI). Bioresour. Technol. 134, 94–100.

Ning, Q.M., Liu, Y.G., Liu, S.B., Jiang, L.H., Zeng, G.M., Zeng, Z.W., Wang, X.H., Li, J., Kare, Z., 2017. Fabrication of hydrochar functionalized Fe–Mn binary oxide nanocomposites: characterization and 17β-estradiol removal. RSC Adv. 7, 37122–37129.

Peng, H., Gao, P., Chu, G., Pan, B., Peng, J., Xing, B., 2017. Enhanced adsorption of Cu(II) and Cd(II) by phosphoric acid-modified biochars. Environ. Pollut. 229, 846–853.

Qin, C., Troya, D., Shang, C., Hildreth, S., Helm, R., Xia, K., 2015. Surface catalyzed oxidative oligomerization of 17β-estradiol by Fe^{3+} saturated montmorillonite. Environ. Sci. Technol. 49, 956–964.

Ramesha, G.K., Kumara, A.V., Muralidhara, H.B., Sampath, S., 2011. Graphene and graphene oxide as effective adsorbents toward anionic and cationic dyes. J. Colloid Interface Sci. 361, 270–277.

Ranjithkumar, V., Sangeetha, S., Vairam, S., 2014. Synthesis of magnetic activated carbon/alpha-Fe_2O_3 nanocomposite and its application in the removal of acid yellow 17 dye from water. J. Hazard. Mater. 273, 127–135.
Reddy, D.H.K., Lee, S., 2014. Magnetic biochar composite: facile synthesis, characterization, and application for heavy metal removal. Colloids Surf. A Physicochem. Eng. Asp. 454, 96–103.
Sahu, J.N., Acharya, J., Meikap, B.C., 2010. Optimization of production conditions for activated carbons from Tamarind wood by zinc chloride using response surface methodology. Bioresour. Technol. 101, 1974–1982.
Sevilla, M., Fuertes, A.B., 2009. Chemical and structural properties of carbonaceous products obtained by hydrothermal carbonization of saccharides. Chem. Eur. J. 15, 4195–4203.
Sun, W., Zhou, K., 2014. Adsorption of 17β-estradiol by multi-walled carbon nanotubes in natural waters with or without aquatic colloids. Chem. Eng. J. 258, 185–193.
Sun, J., Lian, F., Liu, Z., Zhu, L., Song, Z., 2014. Biochars derived from various crop straws: characterization and Cd(II) removal potential. Ecotoxicol. Environ. Saf. 106, 226–231.
Sun, Y., Yue, Q., Gao, B., Gao, Y., Xu, X., Li, Q., Wang, Y., 2014. Adsorption and cosorption of ciprofloxacin and Ni(II) on activated carbon-mechanism study. J. Taiwan Inst. Chem. Eng. 45, 681–688.
Sun, X., Cheng, P., Wang, H., Xu, H., Dang, L., Liu, Z., Lei, Z., 2015. Activation of graphene aerogel with phosphoric acid for enhanced electrocapacitive performance. Carbon 92, 1–10.
Swiatkowski, A., Pakula, M., Biniak, S., Walczyk, M., 2004. Influence of the surface chemistry of modified activated carbon on its electrochemical behaviour in the presence of lead(II) ions. Carbon 42, 3057–3069.
Tan, X.F., Liu, Y.G., Zeng, G.M., Wang, X., Hu, X.J., Gu, Y.L., Yang, Z.Z., 2015. Application of biochar for the removal of pollutants from aqueous solutions. Chemosphere 125, 70–85.
Tan, X.F., Liu, Y.G., Gu, Y.L., Xu, Y., Zeng, G.M., Hu, X.J., Liu, S.B., Wang, X., Liu, S.M., Li, J., 2016. Biochar-based nano-composites for the decontamination of wastewater: a review. Bioresour. Technol. 212, 318–333.
Unur, E., 2013. Functional nanoporous carbons from hydrothermally treated biomass for environmental purification. Microporous Mesoporous Mater. 168, 92–101.
Varshney, D., Yogi, A., 2011. Structural and electrical conductivity of Mn doped hematite (α-Fe_2O_3) phase. J. Mol. Struct. 995, 157–162.
Wang, J., Chen, Z., Chen, B., 2014. Adsorption of polycyclic aromatic hydrocarbons by graphene and graphene oxide nanosheets. Environ. Sci. Technol. 48, 4817–4825.
Wang, H., Gao, B., Wang, S., Fang, J., Xue, Y., Yang, K., 2015. Removal of Pb(II), Cu(II), and Cd(II) from aqueous solutions by biochar derived from $KMnO_4$ treated hickory wood. Bioresour. Technol. 197, 356–362.
Wang, B., Jiang, Y., Li, F., Yang, D., 2017. Preparation of biochar by simultaneous carbonization, magnetization and activation for norfloxacin removal in water. Bioresour. Technol. 233, 159–165.
Wu, Z., Zhong, H., Yuan, X., Wang, H., Wang, L., Chen, X., Zeng, G., Wu, Y., 2014. Adsorptive removal of methylene blue by rhamnolipid-functionalized graphene oxide from wastewater. Water Res. 67, 330–344.
Xiao, J., Qiu, L., Jiang, X., Zhu, Y., Ye, S., Jiang, X., 2013. Magnetic porous carbons with high adsorption capacity synthesized by a microwave-enhanced high temperature ionothermal method from a Fe-based metal-organic framework. Carbon 59, 372–382.
Xue, Y., Gao, B., Yao, Y., Inyang, M., Zhang, M., Zimmerman, A.R., Ro, K.S., 2012. Hydrogen peroxide modification enhances the ability of biochar (hydrochar) produced from hydrothermal carbonization of peanut hull to remove aqueous heavy metals: batch and column tests. Chem. Eng. J. 200-202, 673–680.
Yang, G.X., Jiang, H., 2014. Amino modification of biochar for enhanced adsorption of copper ions from synthetic wastewater. Water Res. 48, 396–405.
Zhang, Y., Zhou, J.L., 2005. Removal of estrone and 17β-estradiol from water by adsorption. Water Res. 39, 3991–4003.
Zhao, G., Li, J., Ren, X., Chen, C., Wang, X., 2011. Few-layered graphene oxide nanosheets as superior sorbents for heavy metal ion pollution management. Environ. Sci. Technol. 45, 10454–10462.
Zhao, N., Zhao, C., Lv, Y., Zhang, W., Du, Y., Hao, Z., Zhang, J., 2017. Adsorption and coadsorption mechanisms of Cr(VI) and organic contaminants on H_3PO_4 treated biochar. Chemosphere 186, 422–429.
Zhou, L., Liu, Y., Liu, S., Yin, Y., Zeng, G., Tan, X., Hu, X., Hu, X., Jiang, L., Ding, Y., Liu, S., Huang, X., 2016. Investigation of the adsorption-reduction mechanisms of hexavalent chromium by ramie biochars of different pyrolytic temperatures. Bioresour. Technol. 218, 351–359.
Zhou, Y., Liu, X., Xiang, Y., Wang, P., Zhang, J., Zhang, F., Wei, J., Luo, L., Lei, M., Tang, L., 2017. Modification of biochar derived from sawdust and its application in removal of tetracycline and copper from aqueous solution: adsorption mechanism and modelling. Bioresour. Technol. 245, 266–273.
Zhou, Q., Liao, B., Lin, L., Qiu, W., Song, Z., 2018. Adsorption of Cu(II) and Cd(II) from aqueous solutions by ferromanganese binary oxide-biochar composites. Sci. Total Environ. 15, 115–122.
Zhu, X., Liu, Y., Qian, F., Zhou, C., Zhang, S., Chen, J., 2014. Preparation of magnetic porous carbon from waste hydrochar by simultaneous activation and magnetization for tetracycline removal. Bioresour. Technol. 154, 209–214.